NASA CR 152365

A COMPARISON OF FLIGHT AND SIMULATION DATA FOR THREE AUTOMATIC LANDING SYSTEM CONTROL LAWS FOR THE AUGMENTOR WING JET STOL RESEARCH AIRPLANE

B. Feinreich and G. Gevaert
Lear Siegler, Inc.
Astronics Division, Santa Monica, CA

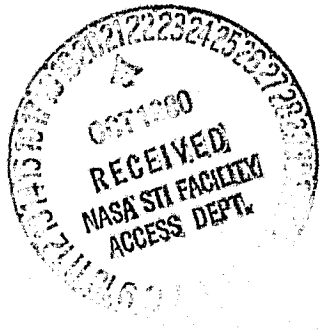

Abstract

The extensive technology base which exists for automatic flare and decrab control laws for conventional takeoff and landing aircraft has been adapted to the unique requirements of the powered lift STOL airplane. Three longitudinal autoland control laws were developed. In addition to conventional controllers, direct lift and direct drag control were used in the longitudinal axis. A fast time simulation was used for the control law synthesis, with emphasis on stochastic performance prediction and evaluation. Through iterative refinements, good correlation with flight test results was obtained. This simulation was used to extrapolate the statistical landing data base beyond the two sigma level established in flight to the improbable level required by the FAA for certification. Excellent touchdown sink-rate control was obtained, with range accuracy consistent with Cat III performance requirements.

Introduction

The Ames Research Center of NASA is conducting a series of investigations to generate and verify through ground based simulation and flight research a data base to aid in the design and certification of advanced propulsive lift short takeoff and landing (STOL) aircraft. One portion of this program is concerned with obtaining technical information on automatic landing systems for STOL aircraft including flight path control performance and touchdown state dispersion in the presence of environmental distrurbances. As part of this program, Lear Siegler's Astronics Division developed automatic landing control laws for the Augmentor Wing Jet STOL Research Airplane.

The technology for the development and certification of Category III automatic landing systems for conventional takeoff and landing (CTOL) jet transports is well developed and documented, as noted in references 1 to 3 for one commercial aircraft and reference 4 for FAA requirements. No comparable technology exists for automatic landing systems for STOL airplanes in general and for powered lift STOL airplanes in particular.

The objective of the automatic landing work reported here is to gain understanding of the problems impacting the design of powered lift short-haul airplanes that are to be landed automatically on STOL runways in adverse weather conditions. This understanding was attained by a limited coverage of important elements that are normally included in the certification process of a CAT III automatic landing system for CTOL airplanes with major emphasis on fault-free performance. The control law development concentrated on the final approach to touchdown phase of the landing, with the majority of the effort expended on longitudinal and vertical control because this is where the peculiarities of the powered-lift STOL vehicle are most prominent.

The development and flight validation of the automatic landing system control laws was conducted in three phases. In the first phase, reported in reference 5, Lear Siegler developed both longitudinal and lateral candidate autoland control laws for a powered lift STOL airplane using an Augmentor Wing Jet STOL airplane as an example. This development was based on previous company experience with automatic landing system designs and on control strategies which were emerging from manual operation of the Augmentor Wing airplane by NASA pilots. For discussion of these manual operations, see reference 6.

In phase 2, candidate automatic landing control laws were selected by NASA for implementation. NASA personnel supervised the development and qualification of the flight software on the airborne hardware simulation resident at the Ames Research Center, conducted the flight testing and analyzed the performance of these control laws.

As the flight program progressed, models and control laws were refined in a joint effort of Lear-Siegler and NASA, culminating in the configurations presented in this report.

Although a lateral control law was flight qualified and evaluated, the main thrust of the program remained on the longitudinal control laws. Three longitudinal control laws emerged for comparison. The primary emphasis in all three longitudinal laws was on achieving an accurate touchdown sink-rate with secondary emphasis on touch-down range dispersion.

In the third phase of the program, Lear Siegler used the results of the NASA flight testing to validate a high speed analog simulation which was then used to generate a large statistical data base to establish the automatic landing system performance at the 10^{-6} probability (improbable event) level.

This paper describes the development of a family of automatic landing system control laws and shows that this type of control law is capable of meeting requirements like those applied by the FAA to CTOL automatic landing systems. The results presented in this paper are derived from both simulation and flight data. A comparison of flight and simulation establishes the validity of the simulation both as a design tool and as a mechanism for extrapolating the flight data to the improbable event.

The Research Airplane and the Approach Conditions

The Airplane

The Augmentor Wing airplane shown in Figure 1 is a modified de Havilland C-8A Buffalo airplane with the wing span reduced to increase wing loading.

This airplane is equipped with jet augmentor flaps as shown in Figure 2, incorporating flow blocking devices called chokes, has drooped ailerons with boundary layer control and incorporates full span leading edge slats. The two original turboprop engines were replaced by two Rolls Royce Spey 801 split flow turbo-fan engines which were supplied by the Canadian government as part of the joint program between NASA Ames Research Center and the Canadian Department of Trade, Industry and Commerce. The cold flow from the engines is ducted to the augmentor flaps and ailerons and the hot thrust is vectorable through the conical exhaust nozzles. A more detailed description of the aircraft and its characteristics is given in Reference 7.

The Approach Condition

The nominal landing approach conditions are given in Table I.

Table I Nominal Approach Conditions

Airspeed, knots	70
Gross Wight, lbs	43,000
Wing Loading lb/ft^2	49.7
Lift Coefficient	3.0
Flight Path Angle, degrees	-7.5
Augmentor Wing Flaps Deflection, degrees	65
Engine RPM, percent	95
Thrust Diverter Nozzles Deflection, degrees from horizontal	75

The Augmentor Wing Jet STOL Research airplane was flown on a 7.5 degree glideslope at speeds near 70 knots for the final approach. At this low approach speed the airplane operates on the backside of the power curve. Because of this and the near vertical thrust orientation in the approach configuration the most effective control for path is the throttle and the most effective control for speed is the elevator. These characteristics are in sharp contrast to a conventional jet transport where during the approach the path is primarily controlled with the elevator and the speed is primarily controlled with the throttle. Reference 6 contains a more complete discussion of the operating characteristics of the Augmentor Wing airplane.

The Airplane Controls

The Augmentor Wing airplane incorporates four controls that can be used in the longitudinal axis for the control of glidepath and automatic flare. The throttle regulates RPM which in turn regulates hot thrust through the exhaust nozzles and cold thrust through the augmentor flaps. The autothrottle was mechanized to give a lift control authority of +0.1g and -0.07g's about the nominal trim point while observing engine limitations and preserving lift margins. Direct lift control is available through the symmetric actuation of surfaces called chokes which can block the flow through the inboard augmentor flaps. These fast acting chokes, when used, are modulated ±30 percent of full closure about a nominal 30 percent position to provide approximately ±0.1g's of lift authority. When the chokes are used, they are complemented with the throttle to improve overall path control bandwidth at the expense of some overall reduction in powered lift augmentation. The powered lift lost by biasing the chokes must be replaced by increasing the aerodynamic lift through a small increase in approach reference airspeed. The thrust conical nozzles, which can be vectored from 6° to 104° from horizontal are always used to trim engine RPM and for some control configurations are also used as a direct longitudinal force device for short term speed control. As a trim device, the nozzles are adjusted to compensate for temperature and wind in order to maintain the engine RPM in a nominal operating range to provide for both upward and downward path corrections.

The maximum RPM limitation is established to avoid structural damage to the nozzles when the nozzles are down. The minimum RPM is set to maintain a minimum value of lift margin as described subsequently. When used as a longitudinal speed control device, the nozzles have a longitudinal authority of +0.13 and -0.09g's for typical nozzle trim values near 75°. A hydraulic powered elevator is the fourth control which is always used for long term speed corrections and is also used, in the absence of nozzle vectoring, to provide short term speed control.

Roll is controlled with ailerons, spoilers and outboard augmentor flap chokes which are mechanically geared to the wheel. A split segment but otherwise conventional powered rudder is used to control yaw.

A unique characteristic of a powered lift aircraft is that it can approach at speeds below the power off stall speed. In order to provide adequate safety margins, CTOL aircraft use an approach speed of 1.3 times the power off stall speed. For powered lift aircraft this would be an excessive requirement and other means must be used to provide safety margins comparble to that used for the CTOL vehicle. Reference 8 describes a comprehensive study of this problem. On the Augmentor Wing aircraft, a lift margin of 0.4g ensures a safe approach speed. Lift margin is defined as the difference in g's between the trim lift value and the maximum lift available from pitch rotation alone with the throttle held constant. Since the lift margin is a function of speed and thrust, limits must be placed not only on the approach speed but also on the minimum value of engine RPM.

The Avionics System

The airplane is equipped with the STOLAND digital avionics system (Reference 9) providing versatile navigation, guidance, control and display functions.

A microwave landing system was used for approach guidance, providing azimuth, elevation and distance information.

Design and Evaluation Methods

Design and Evaluation Process

The design and evaluation process used in this program includes several of the major elements that constitute the certification process of a CTOL airplane CAT III automatic landing system as reported in references 1 through 3. Figure 3 depicts the major elements and flow paths included in the current program. A simulation is used to define and refine the control laws and verify that they produce acceptable landing performance with environmental distrurbances. Initial flight test results are used to refine control laws and airframe models used in the simulation. When good correlation is established between flight and simulation results, the simulation can be used to expand the limited statistical flight data base ($\approx 10^2$) to the extreme event levels ($\approx 10^6$) required for certification.

Using the simulation, data was taken for various levels of environmental distrubances, airframe variations and system errors, covering a wider range than possible in flight. Probability distributions were generated for all touchdown state variables. Total population probability distributions were obtained by convolving the distributions contributed by the different disturbances.

In two major areas this program was less comprehensive than a full certification program: Heavy emphasis during the control law development was placed on performance with no system failures. Less consideration was given to failure effects and redundancy requirements. The system flown was nonredundant, relying on pilot monitoring to ensure safety.

In a full certification program, correlation between simulation and flight is verified through the collection of actual disturbance data as encountered in flight on a landing by landing basis, inserting the same disturbances in the simulation, and correlating the results for a limited number of landings. This was not done in this program due contract funding constraints. Total population results for a given control law configuration is used for correlation instead.

Simulation

A fast-time simulation was the major tool used in synthesizing and evaluating the automatic landing control laws. Mathematical models of the airframe, controllers, sensors and the environment were assembled and used in the simulation. The normal set of uncoupled, linearized, small perturbation equations of motion were used in separate longitudinal and lateral simulations. Longitudinal dynamics were included in the lateral simulation to the extent necessary to account for the goundspeeds associated with different headwinds. Important nonlinearities were modeled, including lift and drag variations associated with changing nozzle angles (which are not small) and with engine RPM settings; lift, pitching moment, and drag variation due to ground effects.

Controller dynamics were modeled, including rate and position limits and significant hysteresis effects. Special care was taken in accurately modelling engine dynamic. Because the engine is used as the major flight path angle controller and has a strong impact on performance. Engine modelling was based on the identification work described in Reference 10. Separate paths were used for computing cold and hot thrust responses, with different time constants used for thrust increase or decrease.

Sensor dynamics and error models which contribute to landing dispersions were also included, such as radar altimeter dynamics and offsets, and dynamic and static vertical gyro and accelerometer errors. MLS noise was modeled and included in the simulation. Winds, shears and turbulence consistent with the definitions in the FAA Advisory Circular 20-57A (reference 4) were used.

For statistical data collection, the simulation was run in fast time repetitive operation mode, starting at 1000 feet above the runway with the airplane stabilized on the glide-slope or localizer, and terminating at touchdown. The 100 foot approach window states were recorded, as were the touchdown states: vertical and lateral velocity, touchdown point on the runway, and pitch, roll and heading angles.

Hardware Simulation and Flight Tests

The automatic landing control laws were programmed into flight control computer software, with testing and validation on the NASA Ames Research Center real time hardware simulator. This total nonlinear six degrees of freedom simulation includes flight control and display computer hardware and pilot interface. The simulation facility was used to qualify each software revision prior to flight.

Flight tests were conducted by NASA Ames Research Center at Crows Landing Naval Auxillary Landing Field (NALF) in California. The flight test landings were made on a simulated 1700 by 100 feet STOL runway with boundaries painted, in accordance with reference 11, on a longer and wider runway. A microwave landing system was installed. A data collection and reduction system with airborne and ground based elements was used to record flight test results.

Control Laws Description

Longitudinal

The glide slope track and flare control laws that have been developed for the Augmentor Wing airplane are shown in the block diagram of Figure 4. A back side of the power curve control technique is used, controlling flight path angle with engine RPM, augmented by the DLC chokes. The elevator is used for attitude stabilization and control and for long term airspeed trim changes. Short term airspeed deviations are controlled through the use of the conical nozzles which are also used for longitudinal trim control to account for the aerodynamic flight path angles resulting from differing wind components. The trim tables shown in Figure 4 pre-position the throttles, nozzles and pitch attitude, and the closed loop control laws correct for deviations from trim. The trim tables outputs are held constant below 300 feet radar altitude. Raw glide slope deviation, computed from elevation and range information, is combined with vertical acceleration in a complementary filter to produce estimates of glide slope deviation and rate which are used for tracking the glide slope. The output of the radar altimeter is blended with vertical acceleration in another complementary filter to produce a sink rate signal that is used in the flare. The glide slope error is faded out prior to flare initiation. Through the flare, derived sink rate is transitioned from glide slope to radar altimeter based information, minimizing the impact of terrain irregularities. A straight line $h/\dot{h}$ profile from the existing pre-flare sink rate to the desired touchdown value is commanded in the flare.

Vertical path errors generate a throttle position or normal acceleration command which drives engine RPM and DLC chokes in a complementary combination. Engine RPM and throttle position are used as feedbacks for the throttle loop to quicken engine response and minimize the effects of hysteresis in the throttle cables. A lag of about one second is associated with the unaugmented engine RPM response to a throttle position change. The closed loop response of the throttle servo and engine to throttle position command can be approximated by second order dynamics. In flight, with a proper choice of gains, a natural frequency of up to 2.5 radians per second (critically damped) could be obtained; attempts to further increase the bandwidth resulted in ringing primarily due to the low rate capability of the throttle servo which was designed for CTOL applications. The chokes are driven with the error between throttle position command and engine RPM, providing fast normal acceleration while engine response is building up. Variations in throttle bandwidth were used to obtain a desirable mix between engine and choke activity while retaining the same overall bandwidth.

Pitch attitude and rate feedback to the elevator are used in stabilizing attitude. On the glide slope, the pitch attitude command provides long term speed control by summing integrated raw airspeed error with the trim table output. Through the flare, attitude is ramped with decreasing altitude from its pre-flare value to the desired touchdown value. This helps arrest the sink rate and puts the airplane in a proper attitude for touchdown. This form of control law is similar to the technique used by pilots for manual landings of the Augmentor Wing Airplane and manual landing of CTOL aircraft. Pitch rotation starts at a main gear height of 65 feet whereas sink rate flare command starts at 50 feet. The proper phasing between these two events provides a smooth entry into the flare.

Raw airspeed is blended in a complementary filter with longitudinal acceleration to produce an estimate of airspeed error which drives the diverter nozzles. A deceleration command is applied during the flare in order to touchdown at approximately 60 knots.

The control laws described above utilize all four controllers available in pitch; configurations using three and two controllers were also defined and evaluated in flight. This was done in order to establish the tradeoff between landing accuracy obtainable by using all controllers and system simplicity gained by minimizing the number of active controllers. Table II summarizes the allocation of controllers in the different control law configurations.

Table II Controller Allocation

Controllers:	4	3	2
Throttle	γ	γ	γ
Elevator	θ	V,θ	V,θ
Choke	γ	γ	-
Nozzle	V	-	-

The nozzle is used for longitudinal trim control on all configurations. All three control law configurations are shown in Figure 4. For the four-control configuration, $K_{\dot{h}}$ and $K_{V\theta}$ are zero and K_{CH} and K_{VN} are nonzero. For the three-control configuration, $K_{\dot{h}}$ and K_{Vn} are zero and K_{Ch} and $K_{V\theta}$ are non-zero. For the two-control configuration, K_{CH} and K_{VN} are zero and $K_{\dot{h}}$ and $K_{V\theta}$ are non-zero.

Lateral-Directional

Figure 5 is a block diagram of the localizer track and runway alignment control laws. Roll control on the Augmentor Wing airplane is achieved by mechanically linking the aileron, roll spoiler and outboard chokes to the control wheel. The lateral control law output commands a wheel position for roll control. Raw localizer lateral displacement, computed from azimuth angle deviation and range, is blended with cross track acceleration in a complementary filter. Yaw acceleration is also added as an input to the filter in order to convert lateral acceleration at the center of gravity to the value at the localizer antenna, located at the airplane's nose. The estimated localizer deviation and its rate are used to command bank angle. The yaw rate, lateral acceleration and bank angle signals are fed through gains, summed and gain scheduled with dynamic pressure to drive the rudder for yaw stability augmentation and turn coordination.

A forward slip maneuver is used for runway alignment. Beginning at an altitude of 150 feet, an align command is switched into the yaw axis. This reference heading command is reduced from the heading error existing at alignment initiation to zero at 50 feet, yielding an alignment rate which is a function of both initial heading error and aircraft sink rate. The error from the commanded heading trajectory is integrated to maintain the steady rudder required during alignment. In the roll axis, the beam computations are maintained to guide the vehicle along the desired horizontal path, with increased cross track rate gain for better control. A bank command proportional to lagged lateral acceleration is added in align to compensate for sideslip induced cross track acceleration. A roll kicker is switched in at align to provide a predictive bank command based on initial heading error. Bank commands in the localizer track path and in the align path are limited to $\pm 10^{o}$ and $\pm 5^{o}$ respectively, which is ample authority to handle steady cross winds in excess of 15 knots.

Landing Performance Results

Longitudinal.

Figures 6 through 11 show touchdown sink rate and range probability distributions obtained with the simulation for the four, three and two control configurations with flight-test data points superimposed.

The appendix explains how to read these curves for the benefit of the readers who are not familiar with this form of data presentation. The simulation results were taken with limiting winds and shears, limiting turbulence and MLS noise. The curves shown are based on a 70 percent probability of encountering limiting headwinds and 30 percent probability for limiting tailwinds (limiting headwinds have a magnitude of 25 knots and limiting tailwinds are 10 knots). Flight results are based on 31 landings with the four control configuration, 29 landings with three controls and 26 two control landings.

A fairly wide range of ambient conditions were encountered during the flight tests since the flights were conducted over several months of the year and different hours of the day. The distribution of winds measured at a mast near the touchdown zone is shown in figure 12 for the four control configuration tests. Even though the majority of landings were made in light winds, headwinds of up to 15 knots, tailwinds up to 11 knots and crosswinds up to 20 knots were encountered. In this program, correlation of flight test and simulator results on a landing by landing basis was not attempted.

Overall probability distributions obtained in flight are compared with the simulator generated probability distributions. These probability distributions are best compared in terms of their slopes. When making this comparison, steeper slopes are expected in the flight data becuase flying occurred in less than limiting wind conditions. Weight and temperature variations and sensor errors (such as radar altimeter bias) in flight tend to decrease the probability distribution curve slope and reduce the difference between flight and simulation.

The simulator curve of Figure 6 indicates that excellent sink rate control was produced by the four control configuration.

The predicted mean touchdown sink rate is 3.8 fps, the two sigma hard landing sink rate is 5.5 fps and the sink rate at a probability level of 10^{-6} is 7.6 fps, which is well within the allowable maximum sink rate of 12 fps for the Augmentor Wing airplane. The probability distribution slope of the flight test points is somewhat steeper than that obtained in the simulation and this trend is expected as discussed above.

Figure 7 shows the touchdown sink rate results for the three control configuration. Since the vertical channel of the four and three control systems are identical, the performance of the two systems should be similar. Figures 6 and 7 show that the simulation data for the two systems is essentially the same. The flight data for the three control system also has a steeper slope than the simulation data. *

Sinkrate distribution for the two control system is shown in Figure 8. Here the highest tolerable bandwidth in the throttle loop was used but the predicted sink rate probability distribution curve slope is flatter than with the four and three control systems becuase of the reduction in bandwidth associated with this no choke configuration. Here again, the slope in the sink rate probability distribution curve was steeper in flight than in the simulation.

---

* After collecting the three control flight data, an error in implementation of the engine - choke system was discovered. Since the error increased the effective choke gain and reduced the effective engine gain the overall normal acceleration was unchanged as long as the chokes were not driven to their limits. This was the case for the flight data shown in Figure 7. A subsequent simulator check also confirmed that for the disturbances experienced in flight, the existing flight data was valid.

The data point at 6 fps tends to follow the bend in the distribution curve predicted by the simulation.

The touchdown sink rate performance of the three longitudinal control laws is summarized in Table III. The performance of all three control laws is satisfactory in the two sigma area. Good agreement exists between the flight and simulation touchdown sink rate results. The 10^{-6} sink rate performance falls within the 12 fps capability of the airplane for all three configurations. However, the 10^{-6} sink rate performance for the four and three control system is considerably better than that of the two control system.

Figures 9, 10, 11 show the touchdown range distribution results for the same three configurations. Range is referenced to the glide path intercept point (GPIP). GPIP is 80 feet short of the touchdown zone as defined in Reference 11 and painted on the Crows Landing NALF STOL port. Two simulator curves are given in each figure, one showing the probability of landing long and the other for landing short.

For the four controls, the simulation determined mean touchdown point is 310 feet with 400 feet between two sigma land short and two sigma land long as shown in Figure 9. Most of the flight points are in good agreement with the simulation results. This is even true for the top four points which are associated with headwinds in excess of 15 knots, crosswinds between 15 and 20 knots and approaches that were not well stabilized. The crosswind conditions were beyond the design envelope of the system.

The simulation data in Figure 10 for the three control system is essentially the same as the simulation data for the four control system. Again, the flight data correlate well with the simulation data and the flight data shows the expected steeper slope associated with lighter winds. The mean touchdown distance for the three control flight data is 70 feet longer than the mean distance for the four control data.

The simulation data for the two control system shown in Figure 11 predicts nearly the same mean range but a 50 percent increase in the short landing to long landing range spread as compared to the four and three control sytems.

Table III Touchdown Performance Comparison

Variable	Four Control		Three Control		Two Control	
	Flight	Simulation	Flight	Simulation	Flight	Simulation
Sink rate, fps						
mean	3.8	3.8	3.1	3.7	3.3	3.7
two sigma, hard	5.0	5.5	4.3	5.2	5.6	6.2
10^{-6}		7.6		7.4		11.9
Range ft						
mean	250	310	320	300	170	290
two sigma, short	-30	100	150	100	-95	30
two sigma, long	380	500	440	520	400	650
10^{-6} short		-210		-160		-320
10^{-6} long		760		780		1040

Comments: 1) Simulation results are with limiting winds and shears, limiting turbulence and MLS beam noise.
2) Range is measured from the Glidepath Intercept Point.

The slope of the flight data probability curve is in reasonably good agreement with the simulation results but the mean value of the flight data is 120 feet short. Differences in the mean touchdown range values between flight and simulation are probably the results of a residual modeling discrepance coupled with the fact that range is not explicitly controlled.

The touchdown range performance comparison of the three logitudinal control laws is shown in Table III. Good agreement exists between flight and simulation touchdown range results with the exception of the difference in the mean value.

The data contained in Table III includes the kind of performance numbers that are required for CTOL autoland certification. The touchdown ranges shown constitute a large percentage of the 1500 to 1800 foot STOL runway length called for in the planning document for STOL ports (reference 11). Certainly, when there is a premium on reducing the touchdown range dispersion, as is the case for the STOL airplane, the better performance of the four and three control systems is to be preferred. Improvement in touchdown range control may be obtained by commanding a higher touchdown sink rate.

In addition to sink rate and range, pitch attitude is a touchdown parameter of interest. Pitch attitude should be high enough such that the airplane would land on themain wheels prior to allowing the nose wheel to touch the runway but it should not be so high as to allow contact of the lower aft fuselage with the runway. Touchdown pitch attitude was well controlled for the Augmentor Wing Airplane for all three configurations. A 6° mean was obtained with about 1° two sigma dispersion. At the 10^{-6} level, the pitch attitude is well within the -1, +15 degree boundaries determined from this airplane's geometry.

Lateral/directional

Figure 13 shows the lateral touchdown distance distribution obtained with the simulation and in 67 landings in flight. The simulation data was taken with maximum design (15 knots) crosswinds and turbulence. The spread in the lateral touchdown distribution of the flight data is more than double that obtained from the simulation. The extreme deviations to the right of the runway's centerline (beyond 15 feet), shown by flight data, are associated with the system operating near or beyond its limits, with quartering headwinds of more than 20 knots and a left crosswind component up to 20 knots, resulting in rudder limiting in some cases. This, however, does not explain the overall wider lateral touchdown distribution of the flight data which is a result of a problem that has not been pinpointed. Other manifestations of this problem are roll excursions from side to side during alignment and not a very tight localizer track, with excursions over 20 feet occurring quite often even in light wind conditions. This compares with 9 feet on a two sigma basis predicted by simulation. Unfortunately, since the emphasis in this program was on the longitudinal axis, the lateral problems were not pursued far enough to positively identify their source and resolve them.

Conclusions

The following conclusions are drawn from the results of these powered lift STOL automatic landing control law studies.

1. For powered lift STOL aircraft that operate on the backside of the power curve, good normal acceleration control is needed for flight path control. This establishes requirements on both amplitude and bandwidth. For the Augmentor Wing airplane both the engine response and the throttle servo rate limits were marginal. These limitations were partially overcome through the use of the direct lift control chokes.

2. With these automatic landing control laws, the longitudinal distance dispersion of the Augmentor Wing airplane is consistent with STOL port requirements as defined in Reference 11. These control laws also provide excellent sink rate control.

3. The primary requirement placed on the STOL autoland control law development was that precise and soft sink rate control be achieved. This is consistent with the current practice for CTOL Category III autoland systems. Better touchdown range control may be possible if the allowable touchdown sink rate is increased through landing gear design or if the emphasis in the control law design is shifted from primarily sink rate control to a combination of sink rate and range control.

4. Good correlation was obtained in the touchdown range and sink rate data between flight and simulation results through an iterative process of refining mathematical models and control laws per flight test results. Under these conditions, the fast time simulation is effective for extrapolating the limited amount of flight data to account for low probability events. Additional work is needed to obtain similar correlation in the lateral axis.

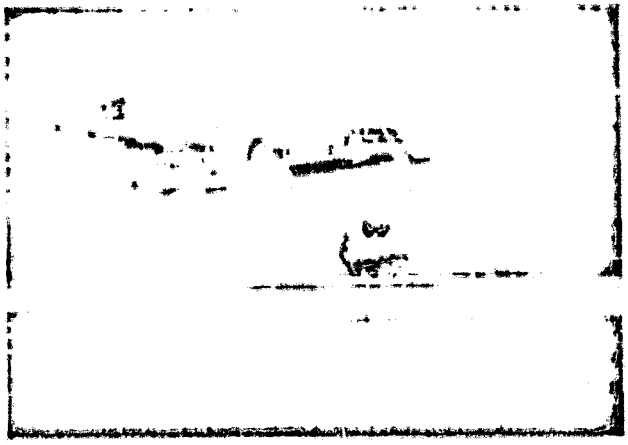

FIGURE 1. THE AUGMENTOR WING AIRPLANE

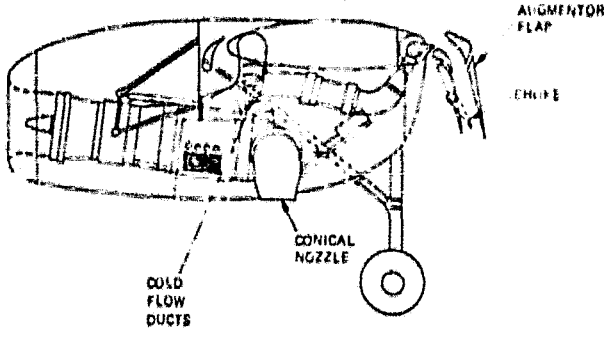

FIGURE 2 ENGINE NACELLE AND CROSS SECTION OF THE JET AUGMENTOR FLAP

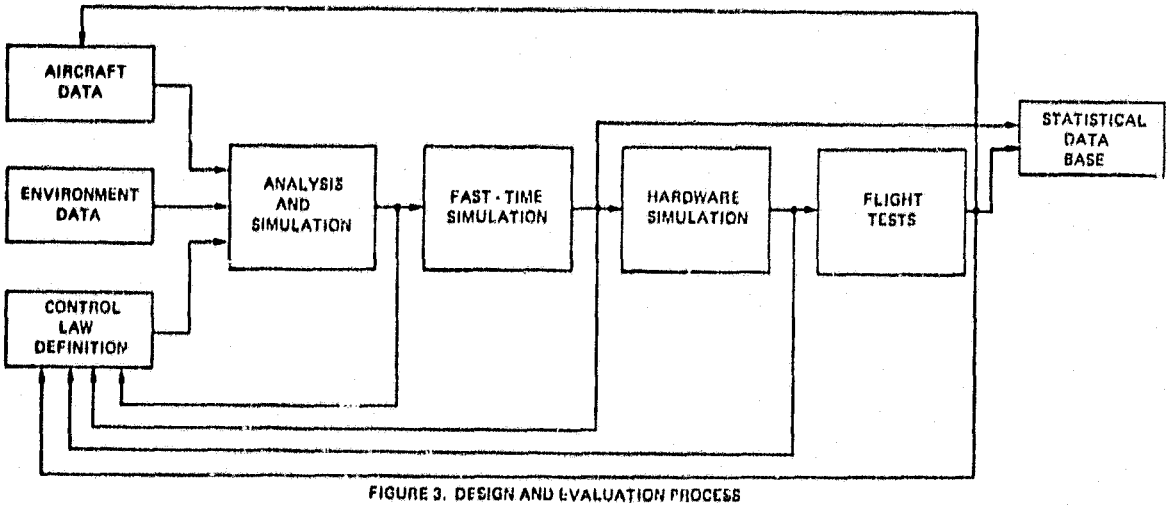

FIGURE 3. DESIGN AND EVALUATION PROCESS

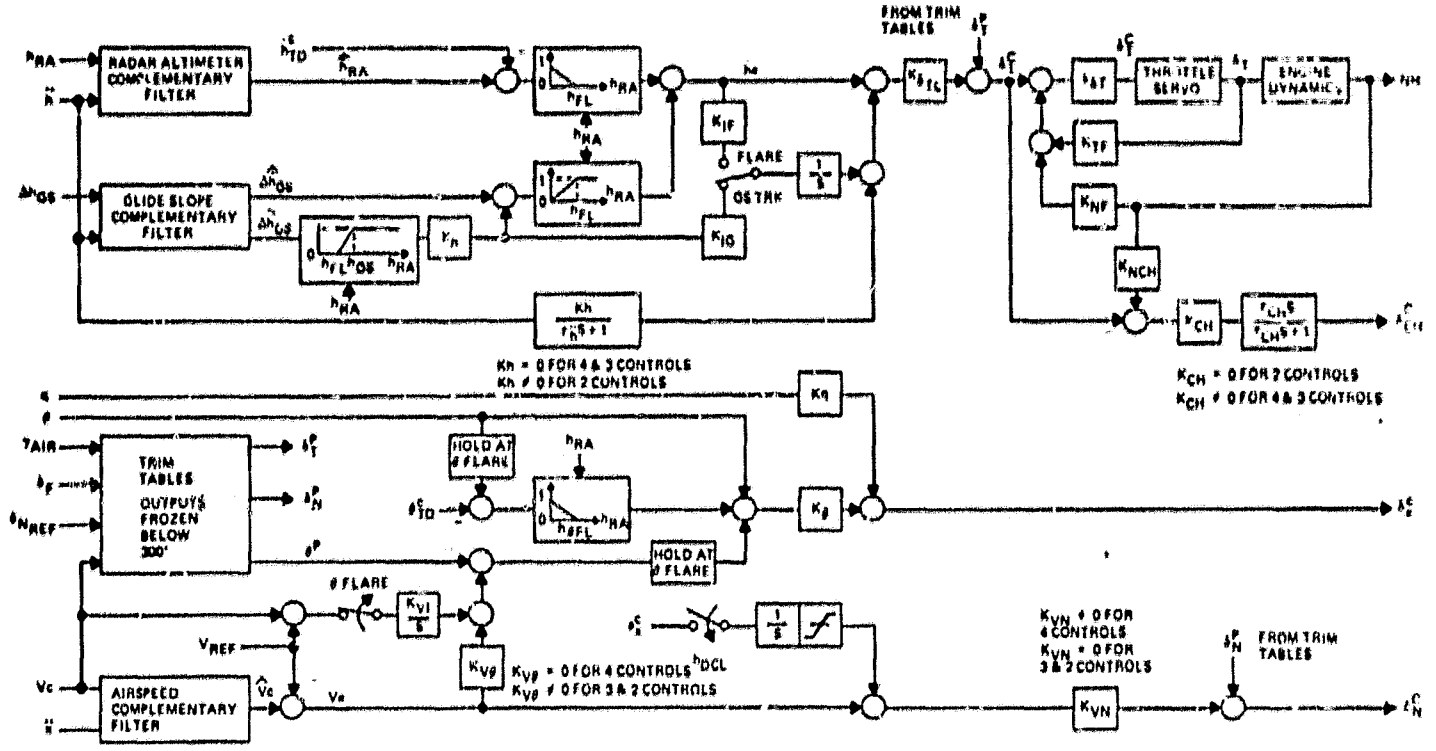

FIGURE 4 GLIDE SLOPE TRACK AND FLARE BLOCK DIAGRAM

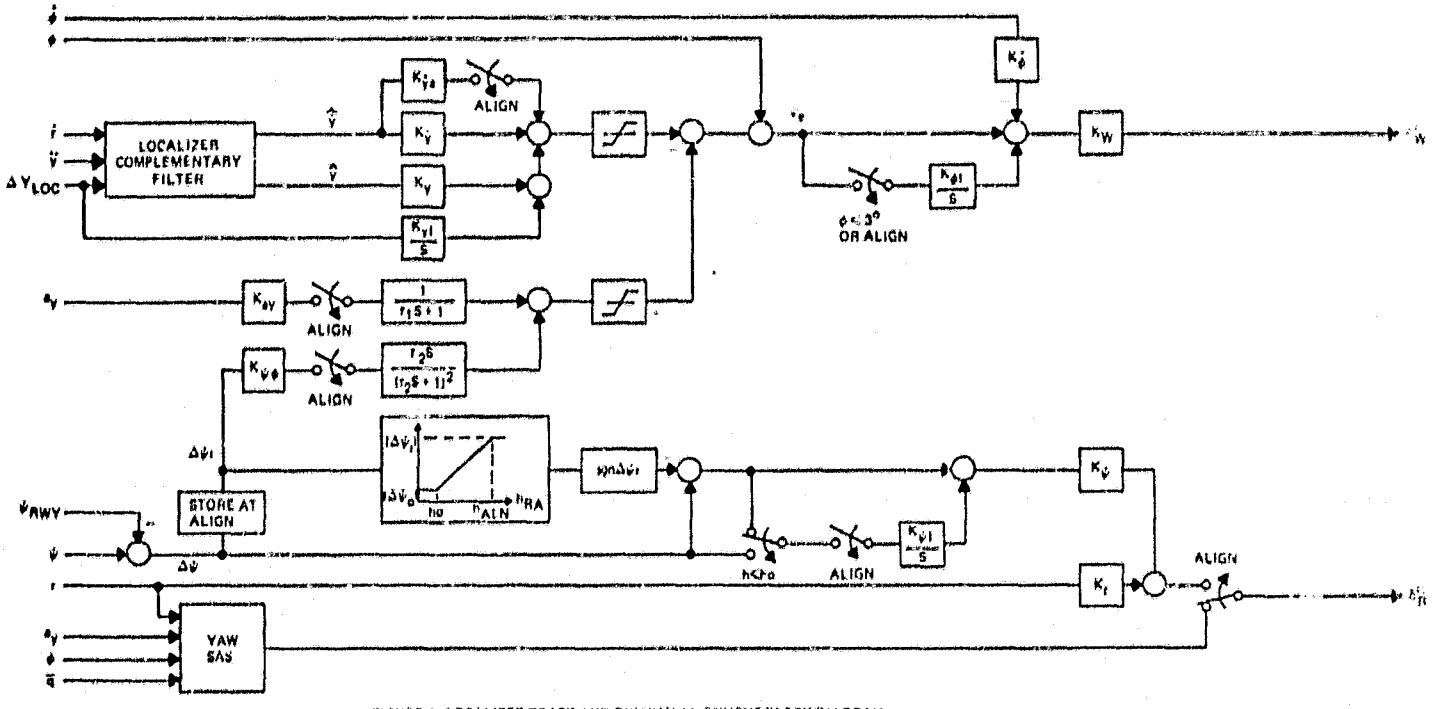

FIGURE 5. LOCALIZER TRACK AND RUNWAY ALIGNMENT BLOCK DIAGRAM

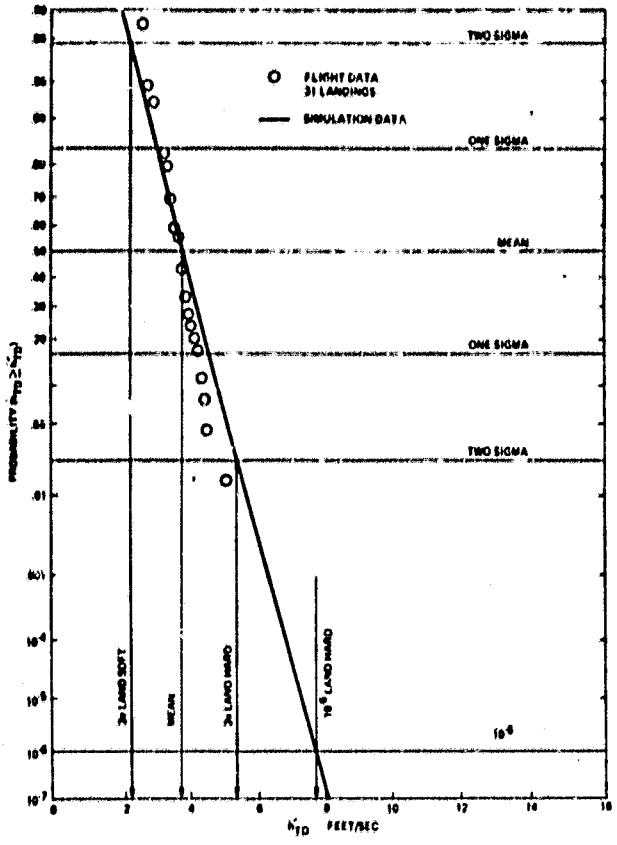

FIGURE 6. TOUCHDOWN SINK RATE DISTRIBUTION, FOUR CONTROLS

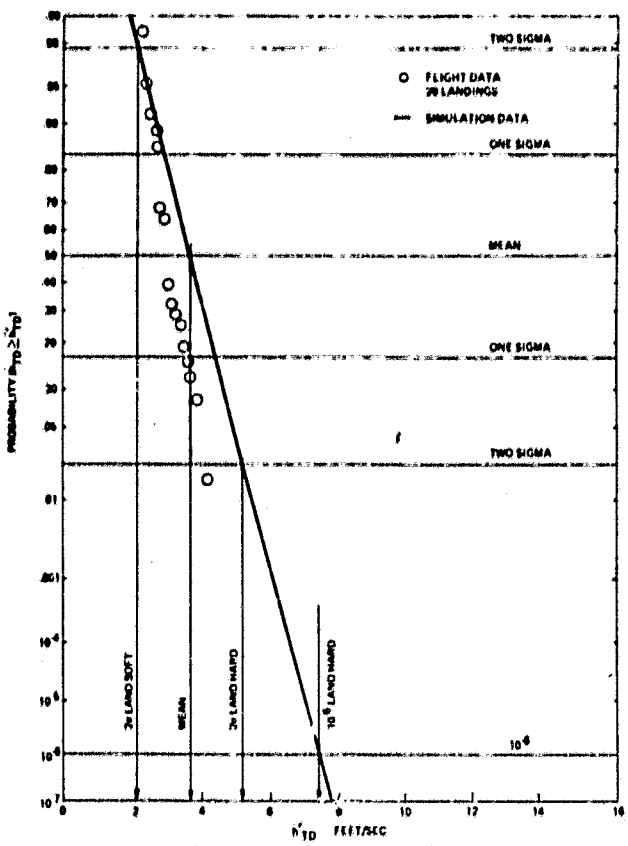

FIGURE 7. TOUCHDOWN SINK RATE DISTRIBUTION THREE CONTROLS

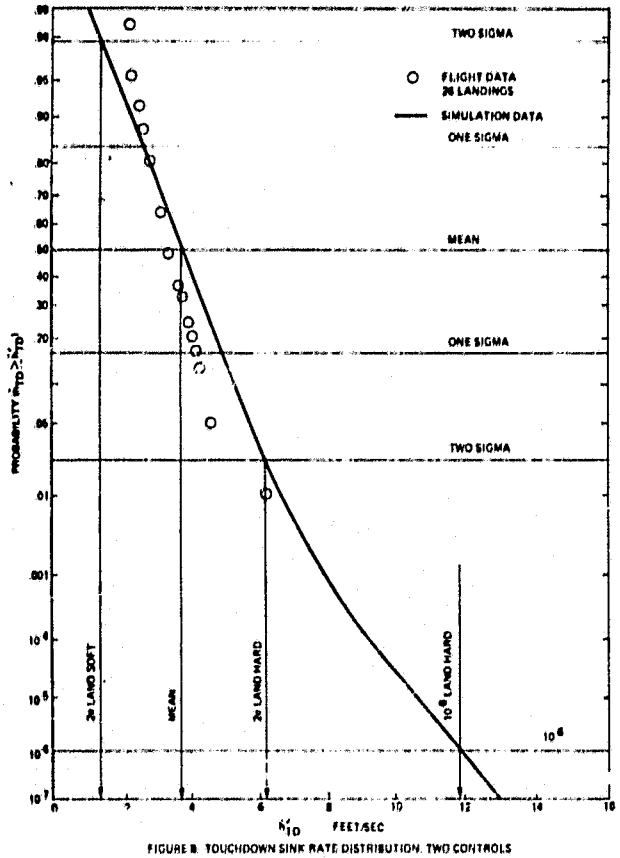

FIGURE 8. TOUCHDOWN SINK RATE DISTRIBUTION, TWO CONTROLS

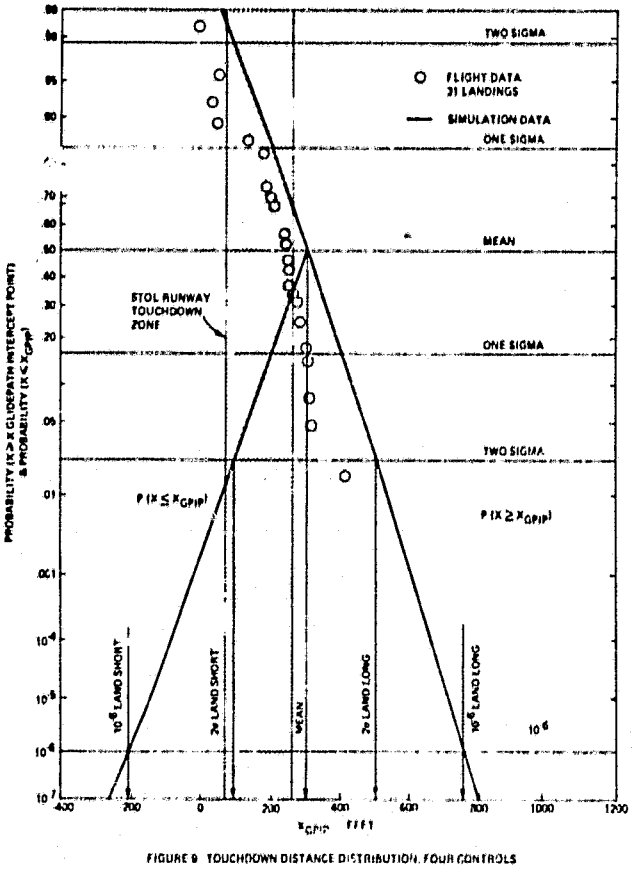

FIGURE 9. TOUCHDOWN DISTANCE DISTRIBUTION, FOUR CONTROLS

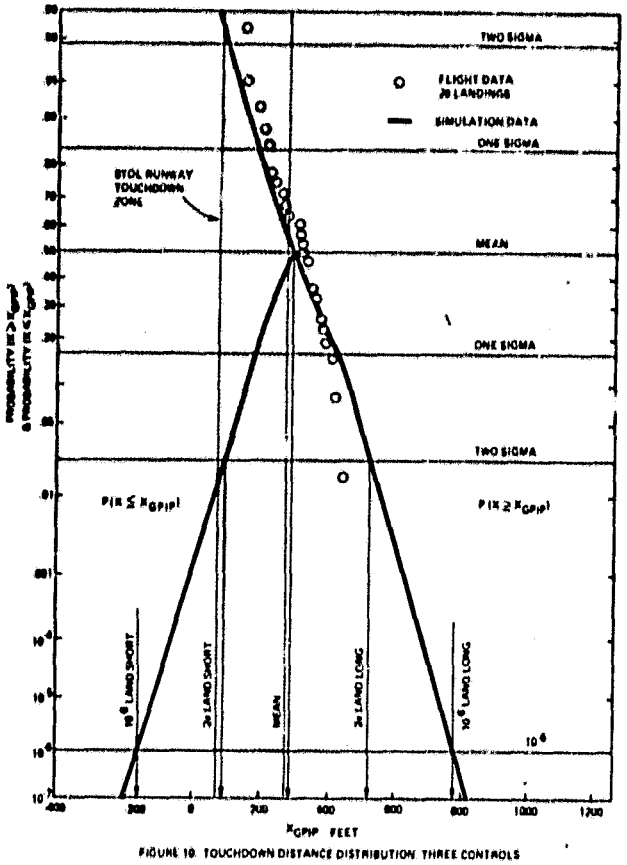

FIGURE 10 TOUCHDOWN DISTANCE DISTRIBUTION, THREE CONTROLS

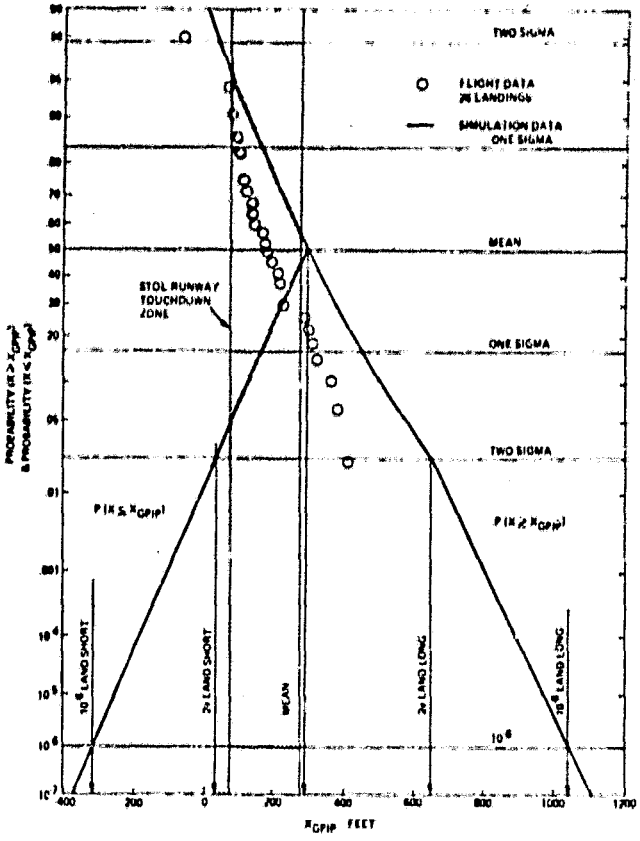

FIGURE 11 TOUCHDOWN DISTANCE DISTRIBUTION, TWO CONTROLS

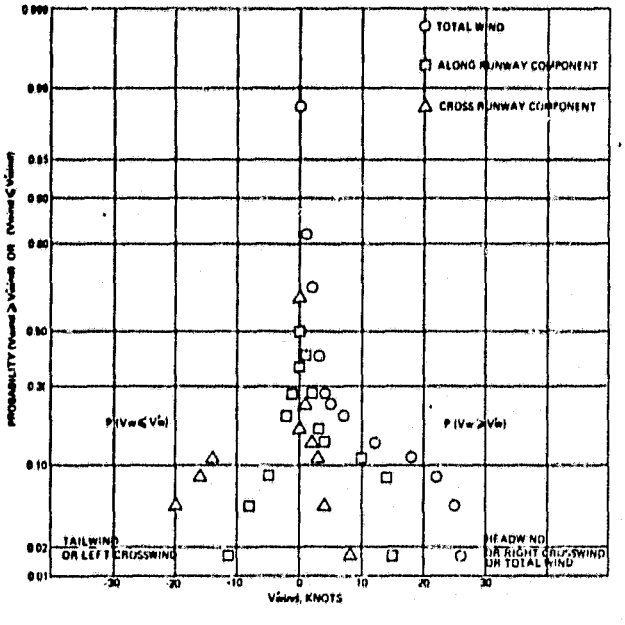

FIGURE 12 WIND DISTRIBUTION, LANDINGS WITH FOUR CONTROLS

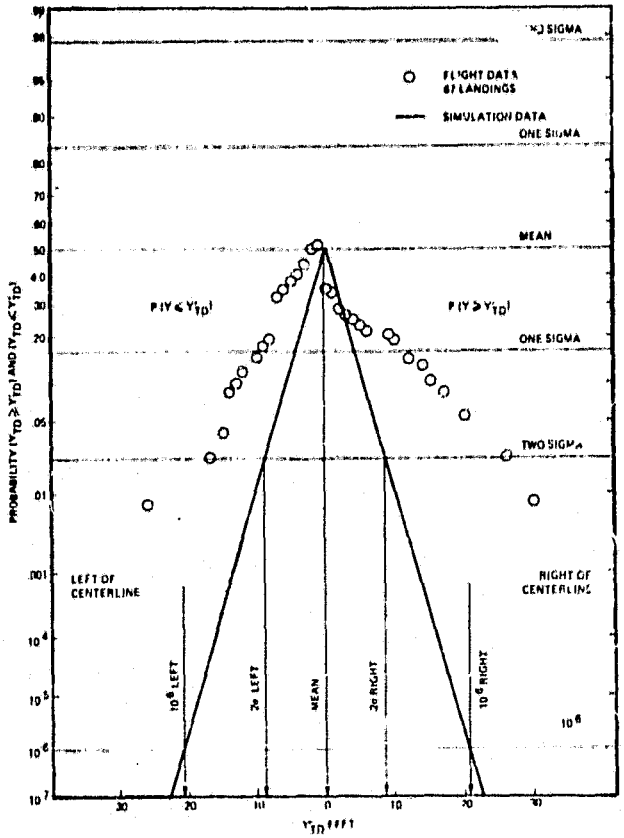

FIGURE 13 LATERAL TOUCHDOWN DISTANCE DISTRIBUTION

References

1. N.M. Shah, G. Gevaert, L.O. Lykken, "The Effect of Aircraft Environment on Category III Autoland Performance and Safety", AIAA 4th Aircraft Design, Flight Test, and Operations Meeting, August, 1972.

2. G. Gevaert, L.O. Lykken, N. M. Shah, "A Simulation Program for Category III Autoland Certification" Summer Computer Simulation Confernece, June 1972.

3. Mineck, D.W., Derr, R.E., Lykken, L.O., Hall, J.C., "Avionic Flight Control System for the Lockheed L-1011 Tristar", SAE Aerospace Control and Guidance Systems Committee Meeting No. 30, September 1972.

4. Anon. "Automatic Landing Systems", FAA, AC 20-57A, 12 January, 1971.

5. Gevaert, G., Feinreich, B., "The development of Advanced Automatic Flare and Decrab for Powered Lift Short Haul Aircraft Using a Microwave Landing System", NASA CR-151948, April 1977.

6. Hindson, W.S., Hardy, G.H., Innis, R.C., "Evaluation of Several STOL Control and Flight Director Concepts from Flight Tests of a Powered-Lift Aircraft Flying Steep, Curved Approaches." NASA TP 1636 (To be published).

7. Quigley, H.C., Innis, R.C., Grosswith, S., "A Flight Investigation of the STOL characterictics of an Augmented Jet Flap STOL Research Aircraft", NASA TM X-62, 334, May 1974.

8. Scott, B.C.; Hynes, C.S.; Martin, P.W.; and Bryder, R.B.: "Progress Toward Development of Civil Airworthiness Criteria for Powered-Lift Aircraft" NASA TMX-73, 124, 1976.

9. Neuman, F., Watson, D.M., Bradbury, P., "Operational Description of an Experimental Digital Avionics System for STOL Airplanes" NASA TM X-62, 448, 1975.

10. De Hoff, R.L., Reed, W.B., Trankle, T.L., Hall, Jr., W.E., "Identification of Spey Engine Dynamics in the Augmentor Wing Jet STOL Research Aircraft from Flight Data" NASA CR-152054, October, 1977.

11. Anon., "Planning and Design Criteria for Metropolitan STOL Ports", FAA Advisory Circular 150/5300-8, November 1970.

SYMBOLS

$\dot{s}_x^C$	Nozzle commanded deceleration rate – fps^2
a_y	Lateral acceleration – fps^2
h_{ALN}	Altitude where runway alignment begins – ft
$\ddot{h}$	Vertical acceleration – fps^2
$\dot{h}_e$	Sink rate error – fps
h_{FL}	Radar altitude at which flare sink rate control begins – ft
h_o	Altitude where runway alignment ends – ft
h_{RA}	Radar altitude – ft
$h_{\theta FL}$	Radar altitude at which the pitch flare maneuver begins – ft
$\dot{h}_{TD}^C$	Commanded touchdown sinkrate – fps
k_{CH}	Choke gain – %/deg
k_h	Glideslope deviation gain – fps/ft
k_{IF}	Flare integrator gain – 1/sec
k_{IG}	Glideslope error integrator gain – 1/sec
k_{NCH}	Engine RPM to choke gain – %/%RPM
k_{NF}	RPM feedback gain – deg/%RPM
k_{TF}	Throttle position feedback gain – deg/deg
k_q	Pitch rate gain – deg/deg/sec
k_r	Yaw rate gain – deg/deg/sec
k_{VI}	Speed integrator gain – deg/sec/fps
k_{VN}	Speed gain to nozzle – deg/fps
$k_{V\theta}$	Speed to pitch gain – deg/fps
k_W	Wheel command gain – deg/deg
k_Y	Lateral position error gain – deg/ft
k_{YI}	Lateral position error integral gain – 1/sec
$k_{\dot{Y}}$	Lateral position rate error gain – deg/fps
$k_{\dot{Y}a}$	Additional lateral position rate error gain at align – deg/fps
$k_{\delta TC}$	Throttle command gain – deg/fps
$k_{\dot{\delta}T}$	Throttle rate command gain – deg/sec/deg
k_θ	Pitch attitude gain – deg/deg
$k_{\phi I}$	Roll integral gain – 1/sec
k_ϕ	Roll rate feedback gain – deg/deg/sec
k_ψ	Yaw feedback gain – deg/deg
$k_{\psi I}$	Yaw error integral gain – 1/sec
$k_{\psi\phi}$	Yaw to roll crossfeed gain at align – deg/deg
NH	High pressure engine RPM – %
q	Pitch rate – deg/sec
$\bar{q}$	Dynamic Pressure – lb/ft^2
$\dot{r}$	Yaw rate – deg/sec
S	Laplace operator
V_C	Calibrated airspeed – fps
$\hat{V}_C$	Filtered calibrated airspeed – fps
V_{REF}	Reference approach airspeed – fps
$\ddot{x}$	Longitudinal acceleration – fps^2

$\hat{Y}$	Filtered lateral position error – ft
$\dot{\hat{Y}}$	Filtered lateral position error rate – ft
$\ddot{Y}$	Lateral acceleration at the c.g. – fps^2
γ_{AIR}	Aerodynamic flight path angle – deg
Δh_{GS}	Glideslope deviation – ft
$\Delta\hat{h}_{GS}$	Filtered glideslope deviation – ft
$\Delta\dot{\hat{h}}_{GS}$	Filtered glideslope deviation rate – fps
ΔY_{LOC}	Lateral position error – ft
$\Delta\psi$	Runway heading error – deg
$\Delta\psi_i$	Heading error when the alignment maneuver begins – deg
$\Delta\psi_o$	Heading error commanded when the alignment maneuver ends – deg
δ^C_{CH}	Choke command – %
δ^C_e	Elevator command – deg
δ_F	Flap position – deg
δ^C_N	Nozzle angle command – deg
δ^P_N	Trim table nozzle command – deg
δ_{NREF}	Reference nozzle position – deg
δ^C_R	Rudder command – deg
δ^C_T	Throttle position command – deg
$\dot{\delta}^C_T$	Throttle rate command – deg/sec
δ^P_T	Trim table throttle command – deg
δ^C_W	Wheel command – deg
θ	Pitch attitude – deg
θ^C_{TD}	Touchdown pitch attitude command – deg
θ^P	Trim table pitch command – deg
τ_{CH}	Choke time constant – sec
$\tau_{\ddot{h}}$	Vertical accelerometer time constant – sec
τ_1	Lateral accelerometer time constant – sec
τ_2	Yaw to roll crossfeed time constant – sec
ϕ	Roll attitude – deg
$\dot{\phi}$	Roll rate – deg/sec
ψ	Heading – deg
ψ_{RWY}	Runway heading – deg

Appendix: Reading Probability Distribution Plots

This paper presents the flight and simulation landing performance results in the form of probability curves plotted on a graph in which a normal probability distribution appears as a straight line. The interpretation of this type of probability plot is presented here for the reader who is unfamiliar with this form of data presentation.

Figure 5 is a curve which shows the probability that the touchdown sink rate exceeds the value shown on the abscissa. In Figure 6, the simulation data probability of landing harder than 2.1 feet per second is 97.7 percent. The probability of landing harder than 5.5 feet per second is 2.3 percent. 2.1 feet per second represents the two sigma probability of landing soft and 5.5 feet per second is the two sigma probability of landing hard. The difference between these soft and hard landing touchdown sink rates is the minus to plus two sigma sinkrate spread and in 95.4 percent of the landings the touchdown sink rate is between these values. Thus, these limits bound the most probable performance of the control system.

In this form of presentation of data, a normal probability distribution appears as a straight line. Non-normal data deviate from a straight line. A very good control system produces data which appear as a near vertical line on the probability graph. The poorer the performance of the system, the more the probability curve leans away from vertical.

In addition to determining the performance of the system for most of the approaches, there is also a requirement to be sure that an unsafe hard landing will be improbable. As a matter of practice, the FAA uses the 10^{-6} probability as the level to be associated with the improbable event. The improbable event touchdown sink rate from Figure 6 is 7.6 feet per second.

In this report, a folded probability curve is used for presenting touchdown distance data. Figure 9 is an example of this form of data presentation. In Fiugure 9, two simulation data probability curves appear. The probability that the touchdown distance exceeds the abscissa values is shown by the solid line to the right of the figure. The probability that the touchdown range is shorter than the ordinate is shown by the solid line to the left of the figure. The curve shown on the left of the figure is obtained from the curve shown to the right by folding the top part of the $P(X \geq X_{GPIP})$ curve vertically around the mean value line. The two sigma short landing distance can be read from either the $P(X \geq X_{GPIP})$ using the upper two sigma line or from the $P(X \leq X_{GPIP})$ curve using the lower two sigma line. This folding of the probability curve about the mean value permits the short landing improbable event value to be read opposite the long landing improbable event value.